

Article

# Electron Beam Induced Enhancement of the Catalytic Properties of Ion-Track Membranes Supported Copper Nanotubes in the Reaction of the P-Nitrophenol Reduction

Anastassiya A. Mashentseva <sup>1,2,\*</sup>, Dmitriy I. Shlimas <sup>1,2</sup>, Artem L. Kozlovskiy <sup>1,2</sup>, Maxim V. Zdorovets <sup>1,2,3</sup>, Alyona V. Russakova <sup>4</sup>, Murat Kassymzhanov <sup>5</sup> and Alexander N. Borisenko <sup>5</sup>

<sup>1</sup> The Institute of Nuclear Physics of the Republic of Kazakhstan, 1 Ibragimov St., Almaty 050032, Kazakhstan

<sup>2</sup> L.N. Gumilyov Eurasian National University, 5 Satpaev St., Nur-Sultan 010008, Kazakhstan

<sup>3</sup> Department of Intelligent Information Technologies, Ural Federal University, 19 Mira St, 620002 Yekaterinburg, Russia

<sup>4</sup> Department “Instrument Engineering and Automation of Technological Processes”, D. Serikbayev East Kazakhstan State Technical University, 69 A.K. Protozanov St., Ust-Kamenogorsk 070004, Kazakhstan

<sup>5</sup> “Park of Nuclear Technologies” JSC, 18/1 Kurchatov St., Kurchatov 071100, Kazakhstan

\* Correspondence: mashentseva.a@gmail.com

Received: 9 August 2019; Accepted: 28 August 2019; Published: 31 August 2019



**Abstract:** This study considers the effect of various doses of electron irradiation on the crystal structure and properties of composite catalysts based on polyethylene terephthalate track-etched membranes and copper nanotubes. Copper nanotubes were obtained by electroless template synthesis and irradiated with electrons with 3.8 MeV energy in the dose range of 100–250 kGy in increments of 50 kGy. The original and irradiated samples of composites were investigated by X-ray diffraction technique (XRD), scanning electron microscopy (SEM) and atomic force microscopy (AFM). The improved catalytic activity of composite membranes with copper nanotubes was demonstrated by the example of the reduction reaction of p-nitrophenol in the presence of sodium borohydride. Irradiation with electrons at doses of 100 and 150 kGy led to reaction rate constant increases by 35 and 59%, respectively, compared to the non-irradiated sample. This enhancing catalytic activity could be attributed to the changing of the crystallite size of copper, as well as the surface roughness of the composite membrane.

**Keywords:** copper nanotubes; composite; track-etched membranes; electron beam irradiation; enhancing catalytic activity

## 1. Introduction

In recent years, the use of ionizing radiation to enhance the structure and properties of nanoscale structures has become one of the promising areas of modern materials science [1]. In addition to the large-scale application in the synthesis of nanoscale structures [2,3], the use of microwave [4], X-ray [5] and gamma radiation [6,7], as well as the processing by accelerated electron beams [8,9] and ions [10] allows directed modification of both the crystal structure and the functional properties of nanomaterials.

One of the promising applications of ionizing radiation is catalysis. Activation of heterogeneous catalysts by high-energy beams can significantly improve their properties. In a number of works, modification of catalysts by gamma rays significantly improved the yield of reactions of oxidative dehydrogenation of propane at the expense of the changes in the concentration of catalytically active

sites on the catalyst surface [11,12]. After the irradiation with gamma rays (0.8 MGy) of the catalysts based on CuO/MgO and NiO/MgO, the rate of decomposition of hydrogen peroxide increased several times [7]. A significant number of studies are devoted to the investigation of the activation process of heterogeneous catalysts by irradiating them with a stream of accelerated high-energy electrons up to 15 MeV generated with the help of an electronic accelerator [13,14]. Under the influence of a beam of accelerated electrons, both on the surface and in the depth of the catalyst, a number of processes take place; they lead to the activation of chemical bonds and the formation of defects on the surface and in the volume of the solid-state body. At the same time, slow electrons (with energy less than 0.15–0.3 MeV) can directly have a chemical impact on the solid-state body and take part in redox reactions. This combined physical and chemical influence of the accelerated electron flux can potentially lead to the formation of new types of active centers [15,16].

Jun et al [17] studied the effect of electron beam irradiation on the catalytic properties of Ni/Al<sub>2</sub>O<sub>3</sub> in the reaction of CO<sub>2</sub>-reforming of methane. The authors showed that the degree of conversion of CO<sub>2</sub> and CH<sub>4</sub> with the formation of H<sub>2</sub> and CO using various catalysts irradiated with an absorbed dose of more than 2 MGy was 5–10% higher than when using an untreated catalyst. In addition, it was found that the concentration of active centers such as Ni<sup>2+</sup> and NiO or surface defects increases with an increase in the dose of absorbed radiation, thereby increasing the conversion rate. Silica-supported titanium dioxide was irradiated in the range of 100–1000 kGy and the photoactivity of this catalyst in the decomposition reaction of azo-dyes increased with the increase in the irradiation dose to 250 kGy [14]. Supported (graphitized carbon, aluminum oxide, titanium) Pd catalysts after the irradiation using an electronic accelerator (1.2–9.0 MGy) were studied in the toluene hydrogenation reaction (in the liquid and gaseous phase). The degree of conversion of toluene in the gas phase reaction increased from 15% to 86.9% for the source and irradiated at a dose of 9.0 MGy of Pd/C catalyst, respectively [18].

During the last decades, composites with enhanced catalytic activity are being studied more and more to meet the practical catalytic performance requirements in the industry of high activity, high selectivity, and good stability [19]. One of the most critical problems for the development of non-supported nanosized catalysts is the need for their separation from reaction media and/or regeneration after every run so a small part of nanoparticles (NPs) can be removed during these manipulations. After the reaction is completed, the heterogeneous magnetic catalyst can accumulate using an external magnet and is subjected to the next cycle [20]. Composite and supported catalysts compared to their colloidal counterparts are being used more and more to meet the practical catalytic performance requirements in the chemical industry, such as high activity and selectivity, as well as reusability and good stability [21]. Thus, development of new composite materials with enhanced catalytic properties has become one of the most relevant tasks for modern material science.

Track-etched membranes (TeMs) with embedded metal nanotubes (NTs) represent a new class of composites with a wide range of practical applications in nanosensorics [22–24], microelectronics [25], material science, and medicine [26,27]. The composite materials based on copper nanotubes or nanowires obtained by electrochemical or electroless deposition into polymer TeMs are the objects of close study in radiation materials science: the effect of accelerated ions [28,29], electrons, and gamma rays [9,30] on the structural and conductive properties of composite membranes has been studied.

It is well-known that electroless template plating represents a technologically modest and highly flexible wet-chemical method for the fabrication of metal films [31]. Metal precipitation selectively occurs on a TeMs substrate surface and is maintained by polymer pre-treatment (sensitization and activation). One of the main advantages of the proposed electroless deposition technique is not only its simplicity, but low cost; this process does not require complicated laboratory equipment and expensive chemicals [32–34]. It is possible to quickly and easily synthesize big samples of composite membranes. Such capacity cannot be achieved using the electrochemical deposition technique, where the dimension of the composite sample depends on the area of the electrodes, the capabilities of the process design, and so on. Polymeric TeMs also have been extensively employed as a stable and excellent nanocatalyst support for synthesizing efficient heterogeneous catalysts for a wide range of

chemical reactions [33,35–38]. TeMs with embedded metallic NTs as highly efficient heterogeneous catalysts have a lot of advantages: a wide range of desired metals/alloys can be easily deposited within the channels of a membrane; the membrane geometry can be prepared with the desired parameters and allowed to uniformly distribute the catalytically-active material over the whole pore's surface; and the possibility to carry out reactions without separation of nanosized catalysts from reaction media after the reaction is complete [39].

Herein, we introduce a facile and reproducible approach to improve the catalytic performance of copper nanotube membranes using accelerated electrons. The effect of the absorbed dose on the catalytic properties of composite membranes by the example of the p-nitrophenol (4-NP) reduction reaction, as well as the effect of crystal planes and sizes, on the catalytic activity was studied. Notably, the as-prepared Cu NTs can be used as an effective catalyst due to their reusability and stability.

## 2. Results

The pristine deposited NTs were grown through the whole polyethylene terephthalate (PET) template and, therefore, had a length of 12  $\mu\text{m}$ . The outer NT diameter approximately corresponds to the pore diameter of the template ( $430 \pm 10$  nm); the inner diameter and wall thickness were determined to be about  $264 \pm 11$  and  $83 \pm 5$  nm, respectively. The surface morphology of the composite membranes and released copper NTs was characterized by scanning electron microscopy (SEM) images as shown in Figure 1.

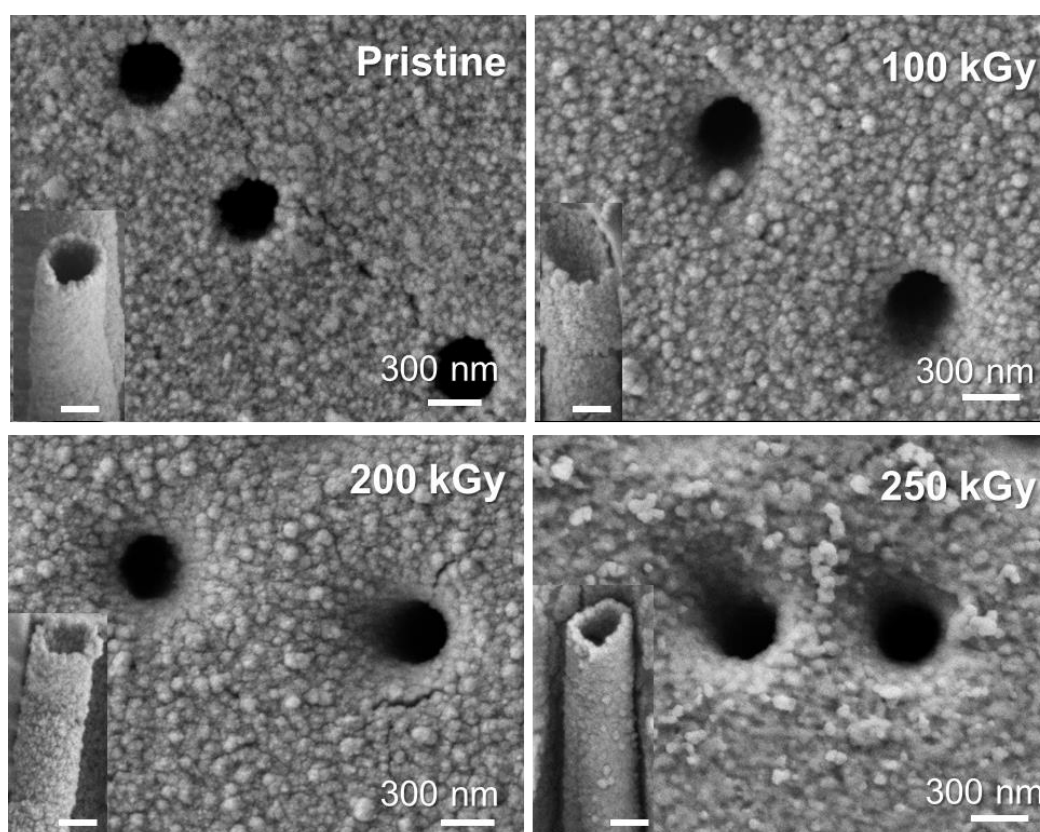


**Figure 1.** Scanning electron microscopy (SEM) images of the composite membrane's surface and individual released Cu nanotubes (inset, scale bar: 200 nm).

According to Figure 1, a uniform layer of copper was deposited in the PET template pores prior to the irradiation treatment. When the composite membranes were irradiated with 100–250 kGy e-beam radiation doses, both lattice distortions and reduction in grain size of the copper nanoparticles (NPs) took place. This led to further agglomeration of NPs in different shapes on the membrane surface,

as well as on NT walls (inset in Figure 1). According to the energy dispersive X-ray spectroscopy (EDS) spectra, Cu is the major component of the prepared nanotubes (99.9%).

The microstructure of the studied samples was analyzed by X-ray diffraction (XRD) and the crystallite size, lattice constants, lattice strain, dislocation density, as well as texture coefficients, were calculated. Figure 2 shows the XRD patterns for different e-beam radiation doses of ion-track composite membranes with embedded Cu NTs. The main distinct XRD peaks for each sample around 43.4, 50.7, 74.3, and 90.0 degrees originated from (111), (200), (220), and (311) planes, respectively.

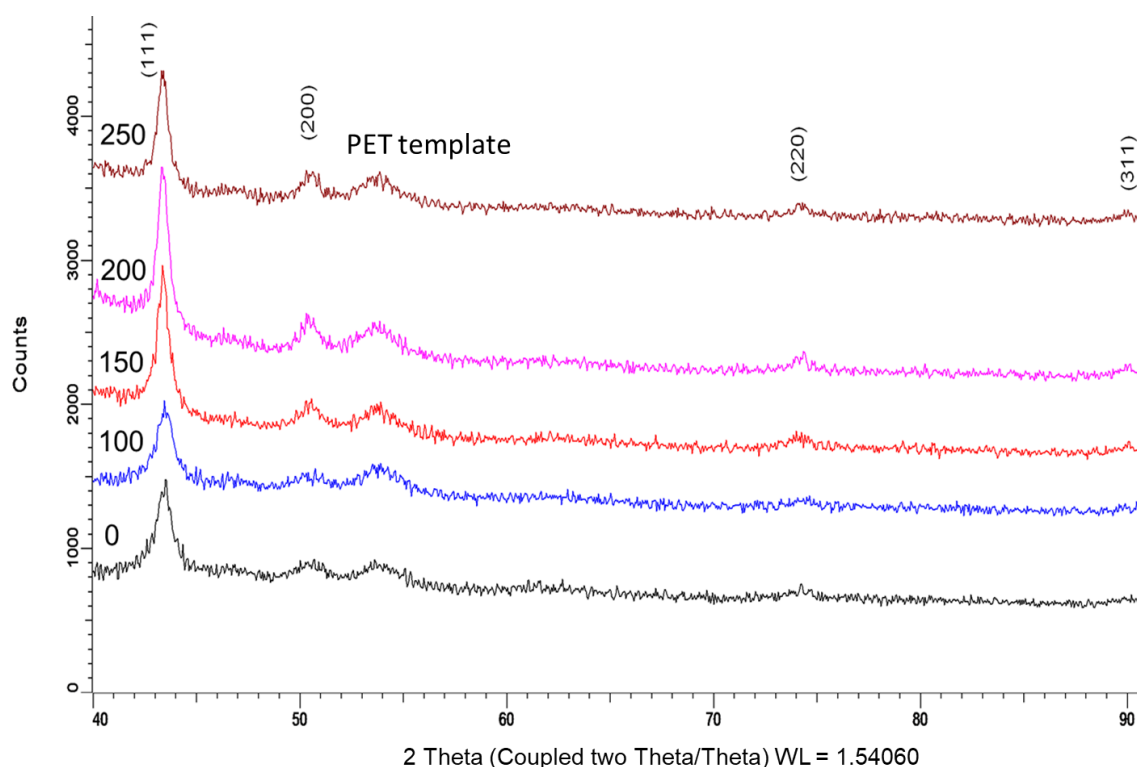


**Figure 2.** X-ray diffraction (XRD) patterns of composite membranes at various e-beam doses.

Initial concentration in the structure plays an important role in the evolution of defects and dislocations. In the chemical synthesis of nanostructures, the concentration of dislocation defects and distortions is quite high, which is due to the way the structure is formed during the nucleation of the tube walls. In this case, the resulting defects and dislocations result in distortion and deformation of the crystal lattice with the formation of disordered regions in the structure. One of the ways to reduce deformations in the structure is the use of ionizing radiation to enhance the properties of nanomaterials. As can be seen from the presented data, the increase in the radiation dose leads to the change in the shape and intensity of the diffraction lines, which indicates the change in distortion and deformation in the crystal structure.

An increase in the radiation dose from 50 to 200 kGy leads to an increase in the intensity of the diffraction peaks (111) and (200), which is due to a decrease in dislocation defects as a result of electron beam irradiation. Changes in the dislocation density of defects and reduction of distortion take place as a result of the formation of electron–positron pairs, followed by the formation of electronic cascades arising from the irradiation by high-energy electrons. Migrating cascades lead to redistribution of defects in the crystal structure and their partial annihilation, followed by changes in structural properties. However, a large concentration of electronic cascades in the structure can result in the disordering of the structure and the formation of amorphous-like inclusions leading to the degradation of the structure, which is observed for the samples irradiated with the dose of 200–250 kGy.

All the peaks observed from XRD patterns can be well indexed to Joint Committee on Powder Diffraction Standards JCPDS card No. 04-0836. It is seen that the deposited pristine and irradiated Cu NTs contain only a copper phase. With the reference to Figure 2 it can be seen that the intensity of the peaks increased up to a higher radiation dose. The XRD parameters of the pristine and e-beam treated PET TeMs with embedded copper NTs are tabulated in Table 1. The crystallite size decreased by 100 kGy and increased with the increase of the e-beam dose from  $10.9 \pm 0.9$  nm by the irradiation of 100 kGy, to  $20.9 \pm 7.5$  by the irradiation of 250 kGy. These changes are caused by the thermal heating effect of the sample that took place during irradiation.

**Table 1.** XRD parameters of the pristine and e-beam treated PET track-etched membranes (TeMs) with embedded copper nanotubes (NTs).

Dose, kGy	Lattice Strain, %	Cell Parameter, $a$ , Å	Crystallinity Degree, %	Texture Coefficient (hkl)			
				111	200	220	311
0	0.325	3.601	57.9	3.225	0.562	0.213	
100	0.293	3.602	64.6	3.655	0.345	1.024	
150	0.211	3.611	65.2	2.461	0.985	0.431	0.123
200	0.134	3.613	71.1	2.168	0.431	0.563	0.245
250	0.121	3.610	72.5	2.478	0.965	0.345	0.212

The decrease in the dislocation density ( $\delta$ ) values (Figure 3) and, consequently, the lattice strain, is caused by an increase in thermal vibrations and the splitting of grains as a result of the interaction of incident electrons with the crystal lattice of copper NTs [9].

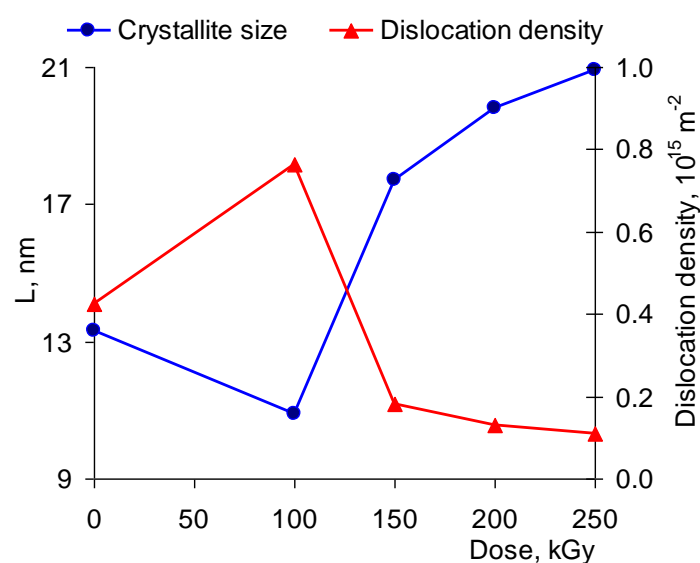


**Figure 3.** Dislocation density and crystallite size variation according to irradiation dose.

The degree of preferred orientation of the synthesized NTs was estimated from the XRD peak intensities using the Harris equation as shown in Equation (1):

$$TC_{hkl} = \frac{I_{hkl}}{I_{0hkl}} \frac{1}{n} \sum \frac{I_{hkl}}{I_{0hkl}} \quad (1)$$

where  $I_{hkl}$  is the experimentally obtained relative intensity,  $I_{0hkl}$  is the relative intensity corresponding to the given plane according to the JCPDS base, and  $n$  is the number of planes.

In our case,  $n = 4$ , as the four most intense reflections were selected (i.e., (111), (200), (220), and (311) peaks). Therefore, for an extremely textured sample, a texture coefficient (TC) would be equal to

4 while the others would be equal to 0; inversely, a fully random oriented sample would have a  $TC_{hkl}$  value equal to 1 for each peak [40]. The obtained values of the TC are listed in Table 1. The copper NTs in the pristine sample have a preferred single orientation along (111) plane direction. After irradiation by up to 100 kGy the  $TC(111)$  and  $TC(200)$  increased sharply. Generally, all irradiated samples display a similar behavior, with  $TC(111)$  in the 2.4–3.6 range, and all other  $TC_{hkl}$  under 1.

The catalytic properties of the studied composite membranes were evaluated by their efficiency in degradation of the p-nitrophenol (4-NP)(Figure 4a). This reaction has a pseudo-first-order under the condition of an excess of reducing agent ( $NaBH_4$ ), which investigates the reaction kinetics by decreasing the amount of the initial reagent [41,42]. In the absence of catalysts, the formation of the final product, p-aminophenol (4-AP) was not observed even with an increase in the reaction time by up to 120 h. The amount of loaded copper NTs was found to be 7.56 mg (0.12 mMol) and was the same for all experiments.

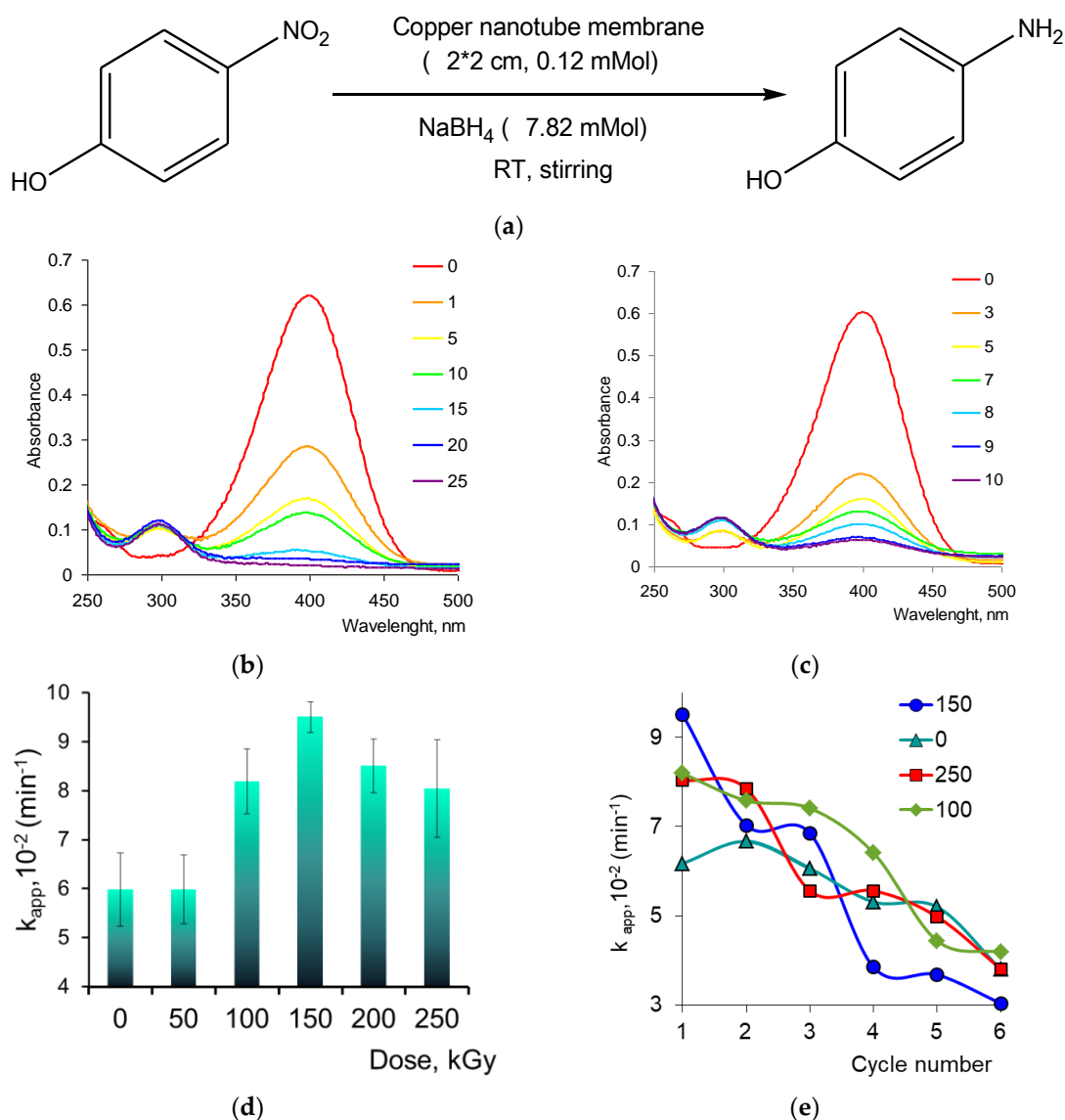


**Figure 4.** Scheme of the studied reaction of the p-nitrophenol reduction (a), typical time-dependent absorption spectra for the catalytic reduction of p-nitrophenol on the surface of the (b) pristine and (c) irradiated (150 kGy) Cu NTs composite membrane; the change of the rate constant for the (d) first run and (e) six consecutive test cycles.

In Figure 4b–d the typical absorption spectra for 4-NP reduction in the presence of composite membranes with embedded copper NTs, as well as the average value of constant rate, are presented (for the first cycle of testing). The analysis of the obtained data on the 4-NP reduction reaction rate constant during the first cycle of tests showed that during electron irradiation there is a significant increase in the catalytic properties of composite membranes by 37.1% and 59.6% at the dose of 100 and 150 kGy, respectively.

Stability and reusability are of great importance for the practical application of catalysts. Porous-supported catalysts bear a number of advantages compared to their counterparts. Non-supported nanoparticles before re-loading have to be separated from solution via filtration, sedimentation, and centrifugation, which are both time-consuming and uneconomic [20]. Flexible TeMs with embedded NTs can be easily removed after reaction and reused again without any additional activation procedure. To evaluate the long-term stability, the activity of the studied composites during six consecutive cycles was analyzed (Figure 4e). As mentioned above, all tests were performed without any additional activation and regeneration procedures. In general, for all the samples there is a slight decrease in the reaction rate constant after the second cycle of tests, and a decrease in activity by more than 50–60% after the sixth cycle. The  $k$  values become approximately the same for the original and irradiated composite membranes. A slight decrease in the reaction rate constant under irradiation at more than 200 kGy is most likely due to the increase in the size of the crystallites of copper [43] and the changes in the surface roughness of the composite membrane [44].

We determined that a pristine sample could establish 95.8–92.1% conversion of 4-NP to 4-AP in up to three consecutive reactions followed by a slightly reduced conversion for the fourth and fifth cycle at 84.6 and 81%, respectively (Figure 5). Meanwhile, the e-beam treated nanocatalyst maintained about 100% conversion for the three consecutive reactions. The most impressive performance was achieved by a 150 kGy nanocatalyst which could maintain 99.3% conversion up to five consecutive reactions and 88% for the sixth run of testing. A slight decrease in the degree of the 4-NP conversion, as well as the catalytic activity decay, seems to result from the loss of nanocatalysts during the intense stirring with a Teflon bar.

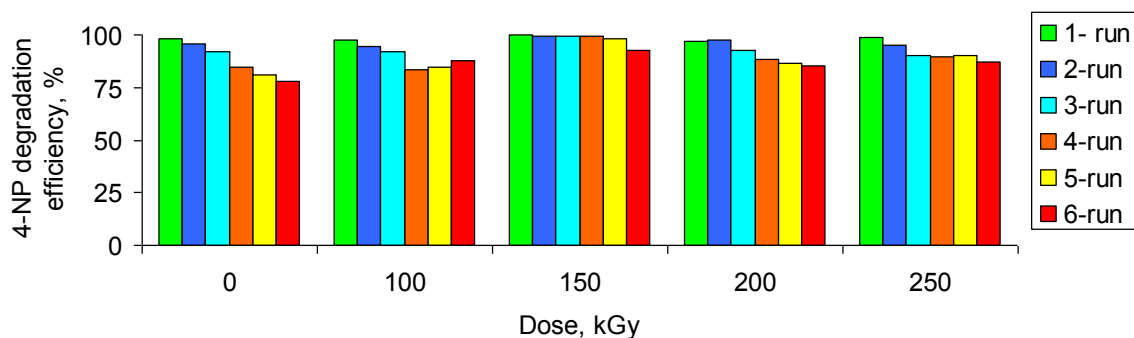


**Figure 5.** Changing of conversion of the 4-NP for six reaction runs in the presence of Cu NTs PET TeMs composite membranes before and after e-beam treatment.

In addition, pre-irradiation by electrons significantly reduced reaction time. For non-irradiated samples the duration of one test cycle was 25–30 min, while for the composite samples after irradiation with a dose of 150 kGy, the reaction was completed within 8–12 min.

For a more detailed study of the effect of high-energy electron irradiation on the structure of composites, the surface topography was investigated by atomic force microscopy (AFM). Generally, AFM analysis is one of the most appropriate techniques used for investigation of materials' surface, especially when surface modification is conducted. AFM analysis was performed at the scan sizes of  $3 \times 3 \mu\text{m}$ , and the dynamics of the surface roughness  $R_a$  for e-beam treated composites was investigated. Figure 6 displays the three-dimensional images acquired from the AFM analysis related to the pristine and e-beam irradiated composite membrane samples. The higher points of the composite membrane

are displayed as bright areas, while the dark areas correspond to the pores. The samples were scanned on a scale of  $3 \times 3 \mu\text{m}^2$  and the calculation of arithmetic average roughness was performed for one image of  $512 \times 512$  points (minimum 10 measurements). The images taken by a scanning probe microscope for each investigated sample are presented in Figure 5 together with information about surface roughness. The parameters of the surface roughness  $R_a$  are also shown in Figure 6.

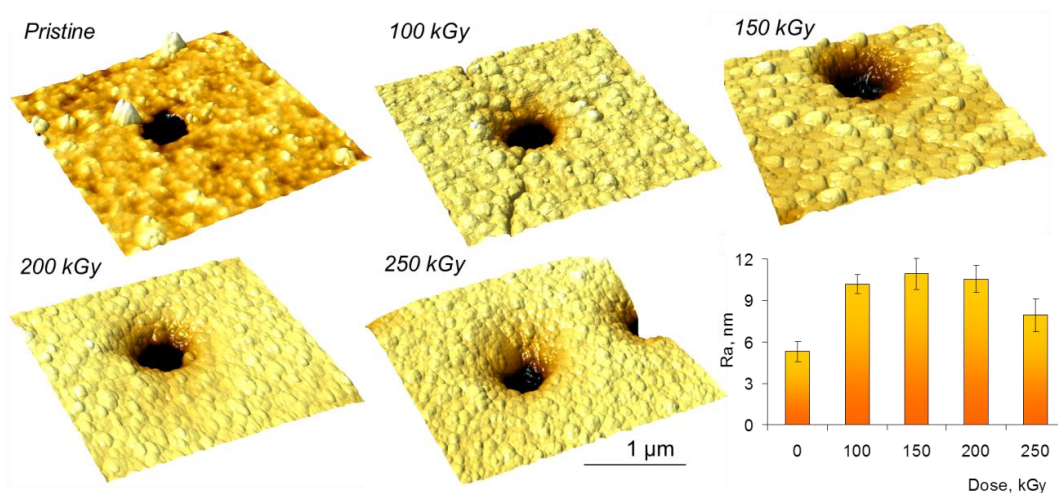


**Figure 6.** Atomic force microscopy (AFM) images of composite membranes with embedded Cu NTs (before and after e-beam irradiation) and the corresponding average value of roughness (inset).

It is well known that the reduction of 4-NP in the presence of  $\text{NaBH}_4$  and nanoscale catalysts proceeds by the Langmuir–Henshelwood mechanism [45], and at the first stage NPs react with the borohydride ions to form metal hydride. Concomitantly, 4-NP is adsorbed, and the rate-determining step consists of the reduction of p-nitrophenol by the metal-hydrogen species. Therefore, the apparent reaction rate can be related to the total surface of a nanosized catalyst. Thus, a significant increase in the values of the roughness of the samples ultimately causes an increased catalytic activity in the 4-NP reduction reaction [46].

Unfortunately, direct comparison with similar results, published in previous reports dedicated to heterogeneous nanosized catalysts for reduction of 4-NP is difficult due to inconsistent reaction conditions, such as the concentration of initial chemicals, the type and size of a loaded catalyst (i.e., NPs, nanowires or NTs), the type of support materials, the range of testing temperature, as well as the mode of testing (cross-flow or bath mode), etc. [36,43]. Thus, the synthesized Cu-P(NIPAM-co-AAc) hybrid microgel as a catalyst for reduction of 4-NP in an aqueous medium for 0.06 to 0.2 mg/L catalyst dosage possesses the  $k$  value in the range of 0.104 to  $0.274 \text{ min}^{-1}$ . The Pd/PdO nanoparticles supported on oxidized multi-walled carbon nanotubes exhibit remarkable catalytic activity during the reduction of 4-NP to 4-aminophenol with the  $k$  value of  $1.0 \text{ min}^{-1}$  [47]. Gold and silver NTs deposited in PET TeMs with a pore density of  $1 \times 10^9 \text{ cm}^{-2}$  exhibit strong catalytic activity with the  $k$  value of  $0.074 \pm 0.02$  and  $0.0447 \pm 0.004 \text{ min}^{-1}$ , respectively. The copper oxide nanoparticles (10 nm) loaded on graphene oxide exhibited promising catalytic activity for the reduction of 4-NP, and the authors successfully reused it for six consecutive cycles with a good yield of 85% after the sixth run [48]. The rate constant for unsupported Cu NPs strongly depends on the shape and size of nanostructures, as well as a synthesis technique and loaded dosage, and is described in more detail in review papers [49–51].

### 3. Materials and Methods

#### 3.1. Chemical Reagents

Copper(II) sulfate pentahydrate, potassium sodium tartrate, palladium chloride, p-nitrophenol, and sodium borohydride made by Sigma, and all other used chemicals had a p.a. or c.p. purity and were used without further purification.

#### 3.2. Template Synthesis of Copper Nanotubes

The polymer template was made of PET film using the DC-60 accelerator of heavy ions (accelerated ion -  $^{15}\text{Kr}^{84}$ , energy of 1.75 MeV/nucleon, film thickness of 12.0 microns, pore density -  $4 \times 10^7$  ion/cm<sup>2</sup>). After the standard procedure of etching in a 2.2 M NaOH solution (260 s), the diameter of the pores of TM according to the method of gas permeability did not exceed  $430 \pm 10$  nm. Sensitization was carried out by rinsing samples for 6 min in a solution containing 50 g/L SnCl<sub>2</sub> and 60 mL/L HCl (37%), after which they were thoroughly washed with hot water for 2–3 min. Further, the sensitized PET TM sample was activated by immersing in the solution of 0.1 g/L PdCl<sub>2</sub> and 10 mL/L HCl (37%) for 6 min. The composition of the deposition solution: KNaC<sub>4</sub>H<sub>4</sub>O<sub>6</sub> × 4H<sub>2</sub>O - 18 g/L; CuSO<sub>4</sub> × 5H<sub>2</sub>O - 5 g/L; NaOH- 7 g/L, CH<sub>2</sub>O - 0.13 M, pH= 12.45 (H<sub>2</sub>SO<sub>4</sub>) [52]; deposition time was 40 min. and temperature was 10 °C. After the completion of the deposition procedure, the samples were washed in ethanol and air dried.

#### 3.3. Electron Irradiation

The as-prepared composite membrane samples were irradiated in the air atmosphere at the electron accelerator ILU-10 (Kurchatov, Kazakhstan). The electron energy value was 3.8 MeV, the average electron beam current was 6.84 mA. The radiation dose was varied by varying the number of runs of the sample holder under the electron beam at a constant speed and was controlled by electronic dosimeters. The dose measurement error did not exceed 10% in all the carried out experiments.

#### 3.4. The Study of the Structure of the Samples

The structure of the samples before and after electron beam irradiation was studied using JEOL JFC-7500F scanning electron microscope. The X-ray diffraction analysis of copper NTs in the polymer matrix was performed in the angular range  $2(\theta)$  20–90° with the step  $2(\theta) = 0.02^\circ$ , and the measurement time was 1 s on the D8 Advance diffractometer (the voltage on the X-ray tube was 40 kV and the current was 40 mA). The average crystallite size was determined by the Scherer equation.

The dislocation density ( $\delta$ ) contains information on the improvement of the crystal structure and was calculated according to the Equation (2).

$$\delta = \frac{1}{L^2} \quad (2)$$

where  $L$  is the crystallite's size.

The distortions taking place in the crystal structure as a result of irradiation can be determined using Equation (3):

$$lattice\_strain = \frac{\beta_{hkl}}{4 \tan \theta} \quad (3)$$

The gas (compressed air was applied) permeability techniques detailed in [53] were used to evaluate the PET TeMs pore sizes and the wall thickness of the resulting NTs. According to the Hagen–Poiseuille Equation (4) the pore size of initial PET TeMs did not exceed  $430 \pm 10$  nm.

$$Q = 4/3(2\pi/MRT)1/2(nr^3\Delta p/l) \quad (4)$$

where  $\Delta p$  is the pressure difference across the membrane,  $M$  is the molecular weight of the gas,  $R$  is the gas constant,  $n$  is the number of nanotubes in the membrane sample (template pores density),  $l$  is the membrane thickness, and  $T$  is the temperature.

The surface morphology of the pristine and irradiated composite membranes was investigated by a scanning probe microscope (SPM) SmartSPM-1000 of AIST-NT company in atmospheric conditions and in the semi-contact mode using a silicon cantilever NSG10 of NT-MDT company, with the tip radius not exceeding 10 nm.

To study the catalytic activity of composite membranes, a  $2 \times 2$  cm sample was placed in 20 mL of the reaction mixture of p-NP ( $7.82 \cdot 10^{-6}$  M) and  $\text{NaBH}_4$  ( $7.82 \cdot 10^{-3}$  M). The study was carried out at continuous stirring at the temperature of  $25 \pm 0.2$  °C; the optical density was measured in the wavelength range of 200–600 nm using the UV-Vis spectrophotometer Specord 250 BU (Jena Analytik, Jena, Germany) every 1–2 min. The reaction rate constant of the first-order, as well as the conversion rate, were determined by changes in the optical density of the initial reagent at 400 nm.

All the experiments were carried out on at least three samples, each sample being tested at least five times; after each cycle the catalyst was washed in deionized water, dried and used further without any additional purification or activation procedures.

#### 4. Conclusions

In this study the copper NTs in the pores of the PET track-etched membrane were synthesized by way of electroless template synthesis. The irradiation of the obtained samples by an electron beam with 3.8 MeV energy and doses of 100–250 kGy was accompanied by some changes in the structure of copper NTs, which was confirmed by XRD studies. When irradiated with a dose of 100 kGy, there is a decrease in the size of crystallites and an increase in the dislocation density of the samples, as well as some change in the texture of copper nanotubes, which in turn has a beneficial effect on the properties of composite membranes. At higher doses, there is a significant increase in the size of the crystallites, a decrease in the lattice strength of copper and an increase in the crystallinity of the samples.

By the example of p-nitrophenol reduction reaction it was shown that high-energy electron irradiation increases the reaction rate by 35–59%, compared to the non-irradiated sample for the first test cycle, and reduces the reaction time by 2–3 times. For the non-irradiated samples, the duration of one test cycle was 25–30 min, while further composite samples after irradiation did not exceed 8–12 min.

The long-term stability properties of the composite catalysts for six consecutive cycles were investigated. It was shown that after four cycles of tests all the samples exhibited equal catalytic activity.

The high surface roughness determined by AFM and several defective sites on the Cu NTs membrane surface resulting from e-beam treatment are believed to be the causes of such high catalytic activity of Cu NTs-based composite membranes irradiated with doses in the range of 100–250 kGy.

**Author Contributions:** Conceptualization, A.A.M. and A.L.K.; data curation, A.V.R.; formal analysis, A.A.M. and M.K.; funding acquisition, M.V.Z. and A.A.M.; investigation, D.I.S., A.V.R. and A.L.K.; methodology, A.A.M. and M.V.Z.; supervision, A.N.B.; writing—original draft, A.A.M. and A.L.K.; writing—review and editing, A.A.M.

**Funding:** A.A.M. gratefully acknowledges the funding of the Ministry of Education and Science of the Republic of Kazakhstan (Project AP05130797).

**Conflicts of Interest:** The authors declare no conflicts of interest.

#### References

1. Wesch, W.; Wendler, E. (Eds.) *Ion Beam Modification of Solids*; Springer Series in Surface Sciences; Springer International Publishing: Cham, Switzerland, 2016; Volume 61, ISBN 978-3-319-33559-9.
2. Gonzalez-Martinez, I.G.; Bachmatiuk, A.; Bezugly, V.; Kunstmann, J.; Gemming, T.; Liu, Z.; Cuniberti, G.; Rummeli, M.H. Electron-beam induced synthesis of nanostructures: a review. *Nanoscale* **2016**, *8*, 11340–11362. [[CrossRef](#)] [[PubMed](#)]

3. Gerasimov, G.Y. Radiation methods in nanotechnology. *J. Eng. Phys. Thermophys.* **2011**, *84*, 947–963. [[CrossRef](#)]
4. Lipińska, T.M.; Borowska, D.; Swędra, N.; Trochim, K. Effect of Microwave Irradiation on the Catalytic Activity of Palladium Supported Catalysts in the One-Step Isomerisation of Cinchona Alkaloids to  $\Delta$ 3,10-Isobases. *Catal. Letters* **2017**, *147*, 2835–2843. [[CrossRef](#)]
5. Chenakin, S.P.; Silvy, R.P.; Kruse, N. X-ray induced surface modification of aluminovanadate oxide. *Catal. Letters* **2005**, *102*, 39–43. [[CrossRef](#)]
6. Gupta, R.; Kumar, R.; Chauhan, R.P.; Chakarvarti, S.K. Gamma ray induced modifications in copper microwires synthesized using track-etched membrane. *Vacuum* **2018**, *148*, 239–247. [[CrossRef](#)]
7. El-Shobaky, G.A.; El-Molla, S.A.; Ismail, S.A. Effects of gamma-irradiation on physicochemical state of surface and catalytic properties of CuO/MgO and NiO/MgO systems. *J. Radioanal. Nucl. Chem.* **2004**, *260*, 627–636. [[CrossRef](#)]
8. Poplavskii, V.V.; Mishchenko, T.S.; Matys, V.G. Ion beam formation of the catalytically active surface of titanium electrodes. *J. Surf. Investig.* **2010**, *4*, 576–581. [[CrossRef](#)]
9. Zdorovets, M.V.; Borgekov, D.B.; Kenzhina, I.E.; Kozlovskiy, A.L. Effect of ionizing radiation on structural and conductive properties of copper nanotubes. *Phys. Lett. A* **2018**, *382*, 175–179. [[CrossRef](#)]
10. Shlimas, D.I.; Kozlovskiy, A.L.; Zdorovets, M.V.; Mashentseva, A.A.; Kadyrzhanov, K.K. Changes in structural and conducting characteristics of zinc nanotubes by bombardment with Xe<sup>+22</sup> heavy ions. *High Energy Chem.* **2017**, *51*, 11–16. [[CrossRef](#)]
11. Khan, M.I.; Aydemir, K.; Siddiqui, M.R.H.; Alwarthan, A.A.; Kaduk, J.A.; Marshall, C.L. Effect of  $\gamma$ -ray irradiation on the properties of nanostructured oxovanadate based oxidative dehydrogenation catalysts. *Radiat. Phys. Chem.* **2013**, *88*, 56–59. [[CrossRef](#)]
12. Ahmad, A.S.; El-Shobaky, G.A.; Al-Noaimi, A.N.; El-Shobaky, H.G. Surface and catalytic properties of gamma-irradiated CuO and NiO catalysts. *Mater. Lett.* **1996**, *26*, 107–112. [[CrossRef](#)]
13. Krashennnikov, A.V.; Nordlund, K. Ion and electron irradiation-induced effects in nanostructured materials. *J. Appl. Phys.* **2010**, *107*. [[CrossRef](#)]
14. Wronski, P.; Surmacki, J.; Abramczyk, H.; Adamus, A.; Nowosielska, M.; Maniukiewicz, W.; Kozanecki, M.; Szadkowska-Nicze, M. Surface, optical and photocatalytic properties of silica-supported TiO<sub>2</sub> treated with electron beam. *Radiat. Phys. Chem.* **2015**, *109*, 40–47. [[CrossRef](#)]
15. Markov, P.V.; Pribytkov, A.S.; Tolkachev, N.N.; Stakheev, A.Y.; Kustov, L.M.; Golubeva, V.N.; Tel'nov, A.V. Effect of electron beam irradiation on the formation of active sites in the Pt/H pentasil catalyst. *Kinet. Catal.* **2008**, *49*, 765–769. [[CrossRef](#)]
16. Pribytkov, A.S.; Tkachenko, O.P.; Stakheev, A.Y.; Klementiev, K.V.; Grunert, W.; Maurits, W.E.V.D.B.; Kustov, L.M.; Golubeva, V.N.; Tel'nov, A.V. Effect of electron beam-irradiation on the structure and catalytic performance of Pd nanoparticles supported on Al<sub>2</sub>O<sub>3</sub> and carbon. *Mendeleev Commun.* **2006**, *16*, 254–256. [[CrossRef](#)]
17. Jun, J.; Kim, J.C.; Shin, J.H.; Lee, K.W.; Baek, Y.S. Effect of electron beam irradiation on CO<sub>2</sub> reforming of methane over Ni/Al<sub>2</sub>O<sub>3</sub> catalysts. *Radiat. Phys. Chem.* **2004**, *71*, 1095–1101. [[CrossRef](#)]
18. Golubeva, V.N.; Pribytkov, A.S.; Tel'nov, A.V.; Baeva, G.N.; Tarasov, A.L.; Telegina, N.S.; Stakheev, A.Y. Effect of electron irradiation on the catalytic properties of supported Pd catalysts. *Kinet. Catal.* **2006**, *47*, 765–769.
19. Xie, Z.; Liu, Z.; Wang, Y.; Yang, Q.; Xu, L.; Ding, W. An overview of recent development in composite catalysts from porous materials for various reactions and processes. *Int. J. Mol. Sci.* **2010**, *11*, 2152–2187. [[CrossRef](#)]
20. Shokouhimehr, M. Magnetically separable and sustainable nanostructured catalysts for heterogeneous reduction of nitroaromatics. *Catalysts* **2015**, *5*, 534–560. [[CrossRef](#)]
21. Munnik, P.; de Jongh, P.E.; de Jong, K.P. Recent Developments in the Synthesis of Supported Catalysts. *Chem. Rev.* **2015**, *115*, 6687–6718. [[CrossRef](#)]
22. Muench, F.; Felix, E.-M.; Rauber, M.; Schaefer, S.; Antoni, M.; Kunz, U.; Kleebe, H.-J.; Trautmann, C.; Ensinger, W. Electrodeposition and electroless plating of hierarchical metal superstructures composed of 1D nano- and microscale building blocks. *Electrochim. Acta* **2016**, *202*, 47–54. [[CrossRef](#)]
23. Wirtz, M.; Parker, M.; Kobayashi, Y.; Martin, C.R. Molecular sieving and sensing with gold nanotube membranes. *Chem. Rec.* **2002**, *2*, 259–267. [[CrossRef](#)] [[PubMed](#)]

24. Hien, V.X.; Minh, N.H.; Son, D.T.; Nghi, N.T.; Phuoc, L.H.; Khoa, C.T.; Vuong, D.D.; Chien, N.D.; Heo, Y.W. Acetone sensing properties of CuO nanowalls synthesized via oxidation of Cu foil in aqueous NH<sub>4</sub>OH. *Vacuum* **2018**, *150*, 129–135. [[CrossRef](#)]
25. Rana, P.; Chauhan, R.P. Size and irradiation effects on the structural and electrical properties of copper nanowires. *Phys. B Condens. Matter* **2014**, *451*, 26–33. [[CrossRef](#)]
26. Hillebrenner, H.; Buyukserin, F.; Stewart, J.D.; Martin, C.R. Template synthesized nanotubes for biomedical delivery applications. *Nanomedicine* **2006**, *1*, 39–50. [[CrossRef](#)] [[PubMed](#)]
27. Choi, Y.; Baker, L.A.; Hillebrenner, H.; Martin, C.R. Biosensing with conically shaped nanopores and nanotubes. *Phys. Chem. Chem. Phys.* **2006**, *8*, 4976. [[CrossRef](#)]
28. Kaliekperov, M.; Kozlovskiy, A.; Shlimas, D.; Kenzhina, I.; Ivanov, I.; Kozin, S.; Aleksandrenko, V.; Kurakhmedov, A.; Sambaev, E.; Seitbaev, A.; et al. The study of changes in structural properties of Cu films under ionizing radiation. *Mater. Res. Express* **2018**, *5*, 055008. [[CrossRef](#)]
29. Zdorovets, M.V.; Mashentseva, A.A.; Kozlovskiy, A.L.; Ivanov, I.A.; Kadyrzhanov, K.K. Ionizing Radiation Induced Modification of the Copper Nanotubes Structure. *J. Nano- Electron. Phys.* **2017**, *9*, 06017. [[CrossRef](#)]
30. Kozlovskiy, A.; Zdorovets, M.; Kaikanov, M.; Kenzhina, I.; Tikhonov, A.V. Systematic Study of Structural and Conductive Properties of Copper Nanotubes Modified By Ionizing Radiation. *Nanosci. Technol. An Int. J.* **2018**, *9*, 139–153.
31. Muench, F.; Rauber, M.; Stegmann, C.; Lauterbach, S.; Kunz, U.; Kleebe, H.-J.; Ensinger, W. Ligand-optimized electroless synthesis of silver nanotubes and their activity in the reduction of 4-nitrophenol. *Nanotechnology* **2011**, *22*, 415602. [[CrossRef](#)]
32. Hulteen, J.C.; Martin, C.R. A general template-based method for the preparation of nanomaterials. *J. Mater. Chem.* **1997**, *7*, 1075–1087. [[CrossRef](#)]
33. Muench, F.; Popovitz-Biro, R.; Bendikov, T.; Feldman, Y.; Hecker, B.; Oezaslan, M.; Rubinstein, I.; Vaskevich, A. Nucleation-Controlled Solution Deposition of Silver Nanoplate Architectures for Facile Derivatization and Catalytic Applications. *Adv. Mater.* **2018**, *30*, 1805179. [[CrossRef](#)] [[PubMed](#)]
34. Muench, F.; Vaskevich, A.; Popovitz-Biro, R.; Bendikov, T.; Feldman, Y.; Rubinstein, I. Expanding the boundaries of metal deposition: High aspect ratio silver nanoplatelets created by merging nanobelts. *Electrochim. Acta* **2018**, *264*, 233–243. [[CrossRef](#)]
35. Yeszhanov, A.B.; Mashentseva, A.A.; Korolkov, I.V.; Gorin, Y.G.; Kozlovskiy, A.L.; Zdorovets, M.V. Copper nanotube composite membrane as a catalyst in Mannich reaction. *Chem. Pap.* **2018**, *72*, 3189–3194. [[CrossRef](#)]
36. Mashentseva, A.A.; Zdorovets, M.V. Catalytic Activity of Composite Track-Etched Membranes Based on Copper Nanotubes in Flow and Static Modes. *Petroleum Chem.* **2019**, *59*, 552–557. [[CrossRef](#)]
37. Mashentseva, A.A.; Zdorovets, M.V. Composites based on polyethylene terephthalate track-etched membranes and silver as hydrogen peroxide decomposition catalysts. *Pet. Chem.* **2017**, *57*, 954–960. [[CrossRef](#)]
38. Sanchez-Castillo, M.A.; Couto, C.; Kim, W.B.; Dumesic, J.A. Gold-Nanotube Membranes for the Oxidation of CO at Gas–Water Interfaces. *Angew. Chemie Int. Ed.* **2004**, *43*, 1140–1142. [[CrossRef](#)] [[PubMed](#)]
39. Mashentseva, A.A.; Zdorovets, M.V.; Borgekov, D.B. Impact of Testing Temperature on the Structure and Catalytic Properties of Au Nanotubes Composites. *Bull. Chem. React. Eng. Catal.* **2018**, *13*, 405. [[CrossRef](#)]
40. Znaidi, L.; Touam, T.; Vrel, D.; Souded, N.; Yahia, S.; Brinza, O.; Fischer, A.; Boudrioua, A. AZO Thin Films by Sol-Gel Process for Integrated Optics. *Coatings* **2013**, *3*, 126–139. [[CrossRef](#)]
41. Pozun, Z.D.; Rodenbusch, S.E.; Keller, E.; Tran, K.; Tang, W.; Stevenson, K.J.; Henkelman, G. A systematic investigation of p -nitrophenol reduction by bimetallic dendrimer encapsulated nanoparticles. *J. Phys. Chem. C* **2013**, *117*, 7598–7604. [[CrossRef](#)]
42. Zhang, K.; Suh, J.M.; Choi, J.-W.; Jang, H.W.; Shokouhimehr, M.; Varma, R.S. Recent Advances in the Nanocatalyst-Assisted NaBH<sub>4</sub> Reduction of Nitroaromatics in Water. *ACS Omega* **2019**, *4*, 483–495. [[CrossRef](#)] [[PubMed](#)]
43. Mashentseva, A.A.; Kozlovskiy, A.L.; Zdorovets, M.V. Influence of deposition temperature on the structure and catalytic properties of the copper nanotubes composite membranes. *Mater. Res. Express* **2018**, *5*, 065041. [[CrossRef](#)]
44. Zhang, W.; Cai, Y.; Qian, R.; Zhao, B.; Zhu, P. Synthesis of Ball-Like Ag Nanorod Aggregates for Surface-Enhanced Raman Scattering and Catalytic Reduction. *Nanomaterials* **2016**, *6*, 99. [[CrossRef](#)] [[PubMed](#)]

45. Wunder, S.; Polzer, F.; Lu, Y.; Mei, Y.; Ballauff, M. Kinetic analysis of catalytic reduction of 4-nitrophenol by metallic nanoparticles immobilized in spherical polyelectrolyte brushes. *J. Phys. Chem. C* **2010**, *114*, 8814–8820. [[CrossRef](#)]
46. Swesi, A.T.; Masud, J.; Nath, M. Enhancing electrocatalytic activity of bifunctional Ni<sub>3</sub>Se<sub>2</sub> for overall water splitting through etching-induced surface nanostructuring. *J. Mater. Res.* **2016**, *31*, 2888–2896. [[CrossRef](#)]
47. Wang, C.; Yang, F.; Yang, W.; Ren, L.; Zhang, Y.; Jia, X.; Zhang, L.; Li, Y. PdO nanoparticles enhancing the catalytic activity of Pd/carbon nanotubes for 4-nitrophenol reduction. *RSC Adv.* **2015**, *5*, 27526–27532. [[CrossRef](#)]
48. Zhang, K.; Suh, J.M.; Lee, T.H.; Cha, J.H.; Choi, J.-W.; Jang, H.W.; Varma, R.S.; Shokouhimehr, M. Copper oxide–graphene oxide nanocomposite: efficient catalyst for hydrogenation of nitroaromatics in water. *Nano Converg.* **2019**, *6*, 6. [[CrossRef](#)]
49. Gawande, M.B.; Goswami, A.; Felpin, F.-X.; Asefa, T.; Huang, X.; Silva, R.; Zou, X.; Zboril, R.; Varma, R.S. Cu and Cu-Based Nanoparticles: Synthesis and Applications in Catalysis. *Chem. Rev.* **2016**, *116*, 3722–3811. [[CrossRef](#)]
50. Ojha, N.K.; Zyryanov, G.V.; Majee, A.; Charushin, V.N.; Chupakhin, O.N.; Santra, S. Copper nanoparticles as inexpensive and efficient catalyst: A valuable contribution in organic synthesis. *Coord. Chem. Rev.* **2017**, *353*, 1–57. [[CrossRef](#)]
51. Duan, Z.; Ma, G.; Zhang, W. Preparation of Copper Nanoparticles and Catalytic Properties for the Reduction of Aromatic Nitro Compounds. *Bull. Korean Chem. Soc.* **2012**, *33*, 4003–4006. [[CrossRef](#)]
52. Mashentseva, A.A.; Kozlovskiy, A.L.; Turapbay, K.O.; Temir, A.M.; Seytbaev, A.S.; Zdorovets, M.V. Determination of Optimal Conditions for Electroless Synthesis of Copper Nanotubes in the Polymer Matrix. *Russ. J. Gen. Chem.* **2018**, *88*, 1213–1218. [[CrossRef](#)]
53. Wirtz, M.; Yu, S.; Martin, C.R. Template synthesized gold nanotube membranes for chemical separations and sensing. *Analyst* **2002**, *127*, 871–879. [[CrossRef](#)] [[PubMed](#)]



© 2019 by the authors. Licensee MDPI, Basel, Switzerland. This article is an open access article distributed under the terms and conditions of the Creative Commons Attribution (CC BY) license (<http://creativecommons.org/licenses/by/4.0/>).